

They are Not Completely Useless: Towards Recycling Transferable Unlabeled Data for Class-Mismatched Semi-Supervised Learning

Zhuo Huang

Ying Tai

Chengjie Wang

Jian Yang

Chen Gong

Abstract

Semi-Supervised Learning (SSL) with mismatched classes deals with the problem that the classes-of-interests in the limited labeled data are only a subset of the classes in massive unlabeled data. As a result, classical SSL methods would be misled by the classes which are only possessed by the unlabeled data. To solve this problem, some recent methods divide unlabeled data to in-distribution (ID) data and harmful out-of-distribution (OOD) data, among which the latter should particularly be weakened. As a result, the potential value contained by OOD data is largely overlooked. To remedy this defect, this paper proposes a “Transferable OOD data Recycling” (TOOR) method which properly utilizes ID data as well as the “recyclable” OOD data to enrich the information for conducting class-mismatched SSL. Specifically, TOOR treats the OOD data that have a close relationship with ID and labeled data as recyclable, and employs adversarial domain adaptation to project them to the space of ID and labeled data. In other words, the recyclability of an OOD datum is evaluated by its transferability, and the recyclable OOD data are transferred so that they are compatible with the distribution of known classes-of-interests. Consequently, our TOOR extracts more information from unlabeled data than existing methods, so it achieves an improved performance which is demonstrated by the experiments on typical benchmark datasets.

1. Introduction

The shortage of labeled data has become a noticeable bottleneck for training many machine learning or computer vision models, as manually annotating a large number of data is usually prohibitive due to the unaffordable monetary cost or huge demand in human resources. A popular way to deal with such a problem is Semi-Supervised Learning (SSL) [8], which effectively harnesses scarce labeled data and abundant unlabeled data to train an accurate classifier.

Classical SSL includes graph-based methods [14, 35, 43], semi-supervised support vector machines [2], co-training [5], and so on. Recently, the research on SSL has made significant progress based on deep neural networks [23] with strong representation ability, and they usually utilize three types of training strategy to handle both

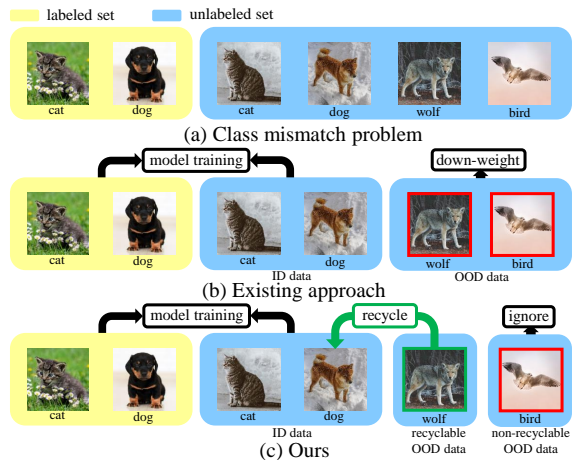


Figure 1. Motivation of our work. (a) Illustration of class mismatch problem. (b) Strategy of existing approaches which utilizes the ID data, meanwhile down-weighting all the detected OOD data. (c) Our method utilizes the ID data as well as the recyclable OOD data, and then ignore the non-recyclable OOD data.

labeled and unlabeled data, namely: 1) *consistency regularization* [19, 22, 26, 28, 33, 42] which enforces that the perturbations on unlabeled data should not change their label predictions significantly; 2) *entropy minimization* [16, 24] which impels networks to make confident predictions on unlabeled data; and 3) *data augmentation* [4, 32, 36, 40] which creates additional examples as well as label information to improve the generalizability of the learned classifier.

However, the above-mentioned SSL approaches rely on a basic assumption that the classes contained by labeled data (*i.e.*, \mathcal{C}_l) and those contained by unlabeled data (*i.e.*, \mathcal{C}_u) are the same, namely $\mathcal{C}_l = \mathcal{C}_u$. Unfortunately, in real-world situations, such assumption is difficult to satisfy as we actually do not know the labels of unlabeled data in advance. Such problem for realistic SSL is called *class mismatch* [30] if some of the classes in unlabeled data are different from those in labeled examples, as shown in Figure 1(a). Concretely, class mismatch means that the classes in labeled data \mathcal{C}_l constitute a subset of the classes in unlabeled data \mathcal{C}_u , namely $\mathcal{C}_l \subseteq \mathcal{C}_u$ and $\mathcal{C}_u \setminus \mathcal{C}_l \neq \emptyset$. Here the unlabeled data that belong to the classes \mathcal{C}_l are called *in-distribution* (ID) data, while the unlabeled data only belonging to \mathcal{C}_u are called *out-of-distribution* (OOD) data. Due to the existence

of OOD data, the traditional SSL methods will be confused and thus generating the degraded test performance regarding the interested classes \mathcal{C}_l .

To solve the class mismatch problem, current works focus on leveraging ID data while trying to weaken the negative impact caused by the OOD data. For example, Chen *et al.* [9] propose a self-distillation method to filter out the probable OOD data based on their confidence scores. Guo *et al.* [17] utilize a weighting mechanism to decrease the influence of OOD data. As shown in Figure 1 (b), both methods regard the rest detected OOD data as substantially harmful that should be discarded [9] or down-weighted [17]. However, here we argue that the detected OOD data are not completely useless, and some of them are informative and can actually be re-used in a suitable way to improve the classification performance. Considering an example, if “dog” and “cat” are two classes of our interests in \mathcal{C}_l to be classified, and the examples of “wolf” and “car” are private in \mathcal{C}_u forming the OOD data. In this case, the unlabeled examples with potential label “wolf” are much more useful than those of “car” in classifying “dog” and “cat” in \mathcal{C}_l , as the appearances of wolf and dog are very similar. As a sequel, they can be activated for our classification task even though they are OOD data. In other words, the prior works [9, 17] tackling class-mismatch problem mostly deploy the selected ID data in unlabeled set, while our method employs both ID data and some useful task-oriented OOD data to train an improved semi-supervised classifier. However, due to the distribution gap between ID data and OOD data, the detected OOD data cannot be directly used for network training, hence we perform a “recycle” procedure to properly re-use the OOD data, which is shown in Figure 1 (c). This is similar to the garbage recycling in our daily life, where the useful part in garbage can be recycled to create extra economic value. Here although the OOD data seem to be useless at the first glance, some of them are still beneficial for SSL training if they are properly used.

Based on the above considerations, this paper proposes a “Transferable OOD Data Recycling” (TOOR) method for SSL under class mismatch which exploits the ID data and simultaneously recycles transferable OOD data in unlabeled set for training a classifier. Specifically, TOOR divides the entire unlabeled set into three subsets in each training round, namely ID data, recyclable OOD data, and non-recyclable OOD data, where only the last subset is discarded for network training. Here ID data are automatically detected according to the fact that the softmax score of ID data would be higher than that of OOD data, while recyclable OOD data and non-recyclable OOD data are decided by evaluating the transferability from them to the feature space of the labeled images. For recyclable OOD data, as their distribution still slightly differs from the labeled data, we propose to conduct domain adaptation through adversar-

ial learning [6, 7, 12, 34, 41] to reduce the potential gap between the two feature distributions. Hence, TOOR is able to learn on more examples than [9, 17] since the transferable OOD data are also well adapted to the space of labeled data to aid SSL training. Thanks to the re-use of transferable OOD data, our TOOR method can be incorporated by many existing SSL approaches (*e.g.*, Mean Teacher [33], VAT [28]) so that class mismatch can be effectively tackled. Comprehensive experiments on typical real-world datasets (*i.e.*, CIFAR10, SVHN, CIFAR100, and ImageNet) reveal that TOOR consistently outperforms other baselines in the presence of mismatched OOD data in the unlabeled set.

2. The Proposed TOOR Approach

This section presents our proposed TOOR approach. In our class-mismatched SSL setting, we use the notations \mathcal{X} and \mathcal{Y} to denote the feature space and label space, respectively. Given a set of training examples $\mathcal{D} = \{\mathbf{x}_i \in \mathcal{X} \subset \mathbb{R}^d, i = 1, 2, \dots, n, n = l + u \text{ with } l \ll u\}$ in which the first l examples are labeled with $\{y_i\}_{i=1}^l \in \mathcal{Y} \in \{1, 2, \dots, c\}$ where c is the number of known classes, and the remaining u examples are unlabeled. We use $\mathcal{D}_l = \{(\mathbf{x}_1, y_1), (\mathbf{x}_2, y_2), \dots, (\mathbf{x}_l, y_l)\}$ to denote the labeled set drawn from the joint distribution P defined on $\mathcal{X} \times \mathcal{Y}$, and $\mathcal{D}_u = \{\mathbf{x}_{l+1}, \mathbf{x}_{l+2}, \dots, \mathbf{x}_{l+u}\}$ to represent the unlabeled set. Particularly, \mathcal{D}_u is assumed to be composed of an ID dataset \mathcal{D}_{id} whose labels are in \mathcal{Y} and an OOD dataset \mathcal{D}_{ood} whose labels are in \mathcal{Y}' with typically $\mathcal{Y} \subset \mathcal{Y}'$, *i.e.*, $\mathcal{D}_u = \mathcal{D}_{id} \cup \mathcal{D}_{ood}$.

The main goal of TOOR is to effectively utilize the class mismatched training set $\mathcal{D} = \mathcal{D}_l \cup \mathcal{D}_u$ to find a semi-supervised classifier that can properly leverage \mathcal{D}_u so that any unseen image \mathbf{x} with unknown true label $y \in \mathcal{Y}$ can be correctly classified. The model of TOOR can be concisely formulated as:

$$\begin{aligned} & \min_{\theta_F, \theta_C} \max_{\theta_D} \underbrace{\frac{1}{l} \sum_{i=1}^l \mathcal{L}_{ce}(C(F(\mathbf{x}_i)), y_i)}_{\text{supervised fidelity term}} \\ & + \lambda \underbrace{\frac{1}{l + |\mathcal{D}_{id}|} \sum_{\mathbf{x}_i \in \mathcal{D}_{id} \cup \mathcal{D}_l} \mathcal{L}_{ssl}(\mathbf{x}_i; \theta_F, \theta_C)}_{\text{ID data exploration term}} \\ & + \gamma \underbrace{\frac{1}{|\mathcal{D}_{ood}|} \sum_{\mathbf{x}_i \in \mathcal{D}_{ood}} w(\mathbf{x}_i) \cdot \mathcal{L}_{adv}(\mathbf{x}_i; \theta_F, \theta_D)}_{\text{OOD data recycling term}} \end{aligned} \quad (1)$$

in which F is an image feature extractor, C is a classifier, D is a discriminator, and θ_F , θ_C , and θ_D are their parameters, respectively. The notation “ $|\cdot|$ ” denotes the size of the corresponding set. In Eq. (1), the first term is dubbed *supervised fidelity term* which involves the standard cross-entropy loss

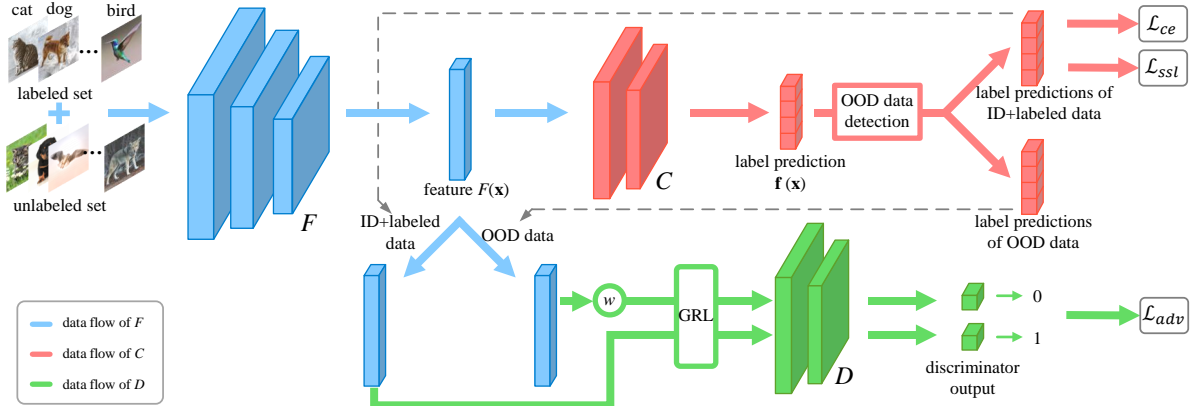


Figure 2. The pipeline of our Transferable OOD data Recycling (TOOR) method, in which F , C and D denote the feature extractor, classifier, and discriminator, respectively. Given the labeled set and unlabeled set, F extracts the feature $F(\mathbf{x})$ for each input image, which is then sent to C to obtain the label prediction vector $\mathbf{f}(\mathbf{x})$ which encodes the probabilities of \mathbf{x} to different classes. Based on $\mathbf{f}(\mathbf{x})$, the OOD data detection module decides whether \mathbf{x} is an ID datum or an OOD datum. Then the determined ID data are used to compute \mathcal{L}_{ce} and \mathcal{L}_{ssl} , and the determined OOD data are further decided to be recyclable or not. Based on the result of OOD data detection, we obtain the features of ID data and OOD data separately (see the gray dashed lines). Finally, the OOD data are weighted by the transferability score $w(\mathbf{x})$, and some of them are recycled by the adversarial learning process composed of the generator F and discriminator D . ‘‘GRL’’ denotes the gradient reversal layer [11] that accomplishes adversarial learning. The above procedure including OOD data detection and adversarial learning for data recycling iterates until all ID data are found and transferable OOD data are recycled.

$\mathcal{L}_{ce}(\cdot)$ to compare the network prediction $C(F(\mathbf{x}_i))$ on every labeled image and its ground-truth label y_i . The second term refers to *ID data exploration term* in which $\mathcal{L}_{ssl}(\cdot)$ denotes the loss defined on ID data and it can be any regularizer in existing SSL method such as consistency regularizer [22, 33] or manifold regularizer [1, 13, 38]. The third term is dubbed *OOD data recycling term* which introduces an adversarial learning loss $\mathcal{L}_{adv}(\cdot)$ to ‘‘recycle’’ the transferable OOD data. Here the OOD data are found by examining their transferability score $w(\mathbf{x}_i)$ which will be detailed in Section 2.2. Through such a recycling procedure, our TOOR approach can maximally exploit class-mismatched datasets without including useless or harmful OOD data, and meanwhile re-use the rich information contained by the transferable unlabeled image examples, leading to superior performance to other methods. The parameters λ and γ are nonnegative coefficients that control the relative weights of the above three terms.

The general procedure of the proposed TOOR algorithm is shown in Figure 2. Given the labeled image set \mathcal{D}_l and unlabeled image set \mathcal{D}_u , we use the feature extractor F to compute the feature representations $F(\mathbf{x})$ for $\mathbf{x} \in \mathcal{D}_l \cup \mathcal{D}_u$. Then, a classifier C is imposed on $F(\mathbf{x})$ to obtain the label prediction vector $\mathbf{f}(\mathbf{x})$ for each of the input images. Based on $\mathbf{f}(\mathbf{x})$, the ID data can be found which are used to compute \mathcal{L}_{ssl} together with the labeled data. The decided OOD data are further sent to the adversarial learning branch so that the recyclable OOD data are called back and the non-recyclable OOD data are completely discarded. Specifically, all OOD data weighted with the transferability scores are combined with the ID data to act as a generator, and they are employed to confuse the discriminator D .

Then D should try its best to distinguish the presented data as ID data (*i.e.*, 1) or OOD data (*i.e.*, 0). During the iterative process between OOD data detection and adversarial learning for recycling, our detected ID dataset expands from the initial limited labeled image set by gradually absorbing the considered ID images and the transferable OOD images. From the above explanations on the procedure of our TOOR, we see that OOD data detection, adversarial learning for recycling, and semi-supervised learning parts are critical in our method, and they will be detailed in Sections 2.1, 2.2, and 2.3, respectively.

2.1. OOD Data Detection

OOD data detection aims to correctly distinguish the unlabeled image data into ID data and OOD data. Many existing works [18, 25] have shown that it can be accomplished by investigating the softmax scores of unlabeled data during network training. Specifically, given an input image \mathbf{x} , its label prediction $\mathbf{f}(\mathbf{x})$ output by the classifier is a c -dimensional vector $[f_1(\mathbf{x}), f_2(\mathbf{x}), \dots, f_c(\mathbf{x})]^\top$, where $\{f_i(\mathbf{x})\}_{i=1}^c$ can be interpreted as the probability that \mathbf{x} belongs to class i . We follow Liang *et al.* [25] to achieve the scaled label prediction $\mathbf{S}(\mathbf{x}; \tau) = [S_1(\mathbf{x}; \tau), S_2(\mathbf{x}; \tau), \dots, S_c(\mathbf{x}; \tau)]^\top$, where $\{S_i(\mathbf{x}; \tau)\}_{i=1}^c$ can be computed as

$$S_i(\mathbf{x}; \tau) = \frac{\exp(f_i(\mathbf{x})/\tau)}{\sum_{j=1}^c \exp(f_j(\mathbf{x})/\tau)}, \quad (2)$$

in which $\tau \in \mathbb{R}^+$ is a temperature scaling [18, 25] parameter that controls the concentration level of the distribution. Here the maximum value of the elements in $\mathbf{S}(\mathbf{x}; \tau)$ is dubbed *softmax score* [25], which is computed as

$$s(\mathbf{x}) = \max_{i \in \{1, \dots, c\}} S_i(\mathbf{x}; \tau). \quad (3)$$

It has been demonstrated in [25] that the softmax scores of ID data are significantly larger than those of OOD data, and thus the softmax scores of different examples can be utilized to judge the unlabeled images as ID or OOD data.

However, in our TOOR approach, due to the aforementioned gradual expansion of ID dataset during the training process, the softmax scores of certain OOD data may oscillate, which make their results of OOD data detection not consistent across successive iterations. To address this problem, we conduct temporal ensembling [22] before the computation of softmax scores to achieve stabilized predictions on all unlabeled data. Concretely, we assemble the label predictions of unlabeled data from historical iterations via using exponential moving average (EMA), which assigns greater weights to recent predictions while exponentially decreasing the weights of early predictions. Therefore, the assembled label prediction of \mathbf{x} is computed as

$$\hat{\mathbf{S}}(\mathbf{x}; \tau)^{(t)} = \eta \hat{\mathbf{S}}(\mathbf{x}; \tau)^{(t-1)} + (1 - \eta) \mathbf{S}(\mathbf{x}; \tau)^{(t)}, \quad (4)$$

where $\mathbf{S}(\mathbf{x}; \tau)^{(t)}$ denotes the scaled label prediction whose elements are computed according to Eq. (2) at the t -th iteration, $\hat{\mathbf{S}}(\mathbf{x}; \tau)^{(t)}$ and $\hat{\mathbf{S}}(\mathbf{x}; \tau)^{(t-1)}$ denote the assembled label predictions at the t -th iteration and the $(t-1)$ -th iteration, respectively. The coefficient $\eta \in [0, 1]$ is a momentum parameter that decides how far the ensemble reaches into training history. Such assembled label prediction $\hat{\mathbf{S}}(\mathbf{x}; \tau)$ varies smoothly and will not be significantly changed across different iterations, which can be used to compute a stabilized softmax score $\hat{s}(\mathbf{x})$ through a similar computation as Eq. (3). Formally, $\hat{s}(\mathbf{x}) = \max_{i \in \{1, \dots, c\}} \hat{S}_i(\mathbf{x}; \tau)$, where $\hat{S}_i(\mathbf{x}; \tau)$ denotes the i -th element of $\hat{\mathbf{S}}(\mathbf{x}; \tau)$. As a result, the stabilized score enables our method to make consistent identification on OOD data.

Given the stabilized softmax score $\hat{s}(\mathbf{x})$, we use a threshold δ to separate OOD data from ID data in the unlabeled set \mathcal{D}_u . Specifically, an image is considered as an ID datum if its stabilized softmax score is larger than δ , and an OOD datum otherwise. Detailed explanation on how δ is chosen is referred to Section 3.3. By introducing $t(\mathbf{x}; \delta)$ as an indication variable regarding \mathbf{x} , this process is formulated as

$$t(\mathbf{x}; \delta) = \begin{cases} 1, & \text{if } \hat{s}(\mathbf{x}) > \delta \\ 0, & \text{if } \hat{s}(\mathbf{x}) \leq \delta \end{cases} \quad (5)$$

That is to say, the images \mathbf{x} 's with $t(\mathbf{x}; \delta) = 1$ are determined as ID data and they will be incorporated by \mathcal{D}_{id} to compute the ID data exploration term in Eq. (1). The experimental results in Section 3.3 show that the computed score can lead to impressive performance.

2.2. Adversarial Learning for Recycling

After detecting the OOD data as mentioned in the above subsection, now we should find the recyclable images in

\mathcal{D}_{ood} and then transfer them to the space of $\mathcal{D}_l \cup \mathcal{D}_{id}$ such that their contained information can be fully extracted for training a semi-supervised classifier. To this end, we treat \mathcal{D}_{ood} as source domain and $\mathcal{D}_l \cup \mathcal{D}_{id}$ as target domain, and propose to use adversarial domain adaptation to achieve this goal. Here we treat $\mathcal{D}_l \cup \mathcal{D}_{id}$ rather than \mathcal{D}_l as target domain as \mathcal{D}_l contains very limited labeled data which cannot faithfully reflect the corresponding distribution and may cause poor generalizability of the obtained classifier. Adversarial domain adaptation [6, 7, 12, 34, 41] aims to learn class discriminative and domain invariant features by using adversarial learning [15]. In our case, the parameters θ_D of the discriminator D are learned to distinguish the previously identified OOD data and ID data by minimizing a cross-entropy loss. Meanwhile, the parameters θ_F of the feature extractor F are trained to deceive the discriminator by maximizing the same cross-entropy loss. In this way, the domain shift between ID data and transferable OOD data is closed, in which the OOD data that are “easily” transferred are likely to be recycled. Hence, by using $\mathcal{D}_l \cup \mathcal{D}_{id}$ as the transfer target, the above adversarial process can be formulated as the min-max game below:

$$\begin{aligned} \min_{\theta_F} \max_{\theta_D} \mathcal{L}_{adv} = & \frac{1}{|\mathcal{D}_{ood}|} \sum_{\mathbf{x}_i \in \mathcal{D}_{ood}} w(\mathbf{x}_i) \log D(F(\mathbf{x}_i)) \\ & + \frac{1}{|\mathcal{D}_{id}| + l} \sum_{\mathbf{x}_i \in \mathcal{D}_{id} \cup \mathcal{D}_l} \log(1 - D(F(\mathbf{x}_i))), \end{aligned} \quad (6)$$

where $w(\mathbf{x}_i)$ is the transferability score that helps to find recyclable OOD data, and the computation of this score will be detailed later. Through such a min-max optimization procedure, the two adversarial opponents converge to a situation where the features of transferable OOD data will be pushed near to the labeled data and ID data, so as to fool the discriminator. Note that we also train the classifier C by minimizing the supervised cross-entropy loss \mathcal{L}_{ce} on the original labeled data, which is simultaneously conducted with adversarial learning. Hence, we can successfully extract the helpful knowledge from OOD data for our classification task on the interested label space \mathcal{Y} .

Here we propose to utilize two cues to find the potential transferable OOD data from the unlabeled set \mathcal{D}_u . Firstly, if the discriminator D cannot tell whether an image $\mathbf{x}_i \in \mathcal{D}_u$ is from the source or target domain, we know that \mathbf{x}_i is quite ambiguous as its representation is close to both ID data and OOD data. Therefore, it is likely to be a transferable image example that should be recycled. To depict this, we introduce a *domain similarity score* $w_d(\mathbf{x}_i)$ for \mathbf{x}_i . Secondly, if the classifier C attributes \mathbf{x}_i to a certain class $y \in \mathcal{Y}$ with a strong tendency, we learn that \mathbf{x}_i probably belongs to this class. To describe this, we introduce a *class tendency score* $w_c(\mathbf{x}_i)$. By adaptively integrating $w_d(\mathbf{x}_i)$ and $w_c(\mathbf{x}_i)$, we acquire the transferability score $w(\mathbf{x}_i)$ for any $\mathbf{x}_i \in \mathcal{D}_u$,

which serves as the weight for \mathbf{x}_i to perform the min-max game in Eq. (6). In the following, we explain the computations for $w_d(\mathbf{x}_i)$, $w_c(\mathbf{x}_i)$ and the integrated $w(\mathbf{x}_i)$.

Domain similarity score $w_d(\mathbf{x}_i)$. Our discriminator D is trained to distinguish ID data from OOD data. The output of discriminator can be interpreted as

$$D(F(\mathbf{x}_i)) = p(\mathbf{x}_i \in \mathcal{D}_{id} \mid \mathbf{x}_i), \mathbf{x}_i \in \mathcal{D}_u, \quad (7)$$

where $p(\cdot)$ denotes probability in this paper. Eq. (7) means that the output value of domain discriminator provides the likelihood of an OOD example \mathbf{x}_i belonging to the domain of \mathcal{D}_{id} . Consequently, if $D(F(\mathbf{x}_i))$ is large, we know that \mathbf{x}_i is similar to the known space of $\mathcal{D}_l \cup \mathcal{D}_{id}$. As a result, we should properly recycle these examples by assigning them large scores. On the other hand, if $D(F(\mathbf{x}_i))$ is small, the corresponding \mathbf{x}_i might not come from the space of $\mathcal{D}_l \cup \mathcal{D}_{id}$. These images should have small scores such that both the discriminator and the classifier will ignore them. Hence, the score reflecting domain information is formulated as

$$\tilde{w}_d(\mathbf{x}_i) = D(F(\mathbf{x}_i)). \quad (8)$$

To obtain more discriminative score assignments across OOD data, we normalize the scores of all unlabeled data to compute domain similarity score, which is

$$w_d(\mathbf{x}_i) = \frac{\tilde{w}_d(\mathbf{x}_i)}{\frac{1}{u} \sum_{j=1}^u \tilde{w}_d(\mathbf{x}_j)}, \mathbf{x}_i \in \mathcal{D}_u, \quad (9)$$

The normalization equipped with the global normalizer helps to enlarge the scores for the potential recyclable OOD data, and meanwhile decreasing the scores of non-transferable OOD data to prevent them from being recycled.

Class tendency score $w_c(\mathbf{x}_i)$. Apart from the domain similarity score, the assembled label predictions of OOD data generated by C also contain rich transferability information. Concretely, the assembled label predictions of ID data can provide valuable clue in evaluating the transferability since the classifier C has been trained on labeled set \mathcal{D}_l and thus possessing considerable discriminability. Hence, inspired by [37], we employ the predictive margin between the largest and the second-largest elements of assembled label prediction vector $\hat{\mathbf{S}}(\mathbf{x}; \tau)$ to establish class tendency score, which is computed as

$$\tilde{w}_c(\mathbf{x}_i) = \max_{j \in \{1, \dots, c\}} \hat{S}_j(\mathbf{x}; \tau) - \max_{k \in \{1, \dots, c\}; k \neq j} \hat{S}_k(\mathbf{x}; \tau). \quad (10)$$

If the predictive margin of an OOD example is large, it implies that the example has relatively large tendency to one certain category, then we consider such OOD examples as transferable data and they could be recycled to the corresponding class j . On the other hand, if the margin is small, which means that the label of this example is quite unclear, it should be excluded for recycling. Similar to the operation on domain similarity score $w_d(\mathbf{x}_i)$, here we also normalize $w_c(\mathbf{x}_i)$ as Eq. (9), which is formulated as

$$w_c(\mathbf{x}_i) = \frac{\tilde{w}_c(\mathbf{x}_i)}{\frac{1}{u} \sum_{j=1}^u \tilde{w}_c(\mathbf{x}_j)}, \mathbf{x}_i \in \mathcal{D}_u. \quad (11)$$

Adaptive integration of $w_d(\mathbf{x}_i)$ and $w_c(\mathbf{x}_i)$. To calculate the transferability scores of all OOD data, we need to combine the obtained domain similarity scores and class tendency scores in a proper way. Specifically, these two scores should be explicitly weighted to yield good performance. By employing the vectors $\mathbf{w}_d = [w_d(\mathbf{x}_1), \dots, w_d(\mathbf{x}_{|\mathcal{D}_{ood}|})]^\top$ and $\mathbf{w}_c = [w_c(\mathbf{x}_1), \dots, w_c(\mathbf{x}_{|\mathcal{D}_{ood}|})]^\top$ to encode the domain similarity scores and class tendency scores for all $\mathbf{x}_i \in \mathcal{D}_{ood}$, here we propose to utilize their variances to compute the trade-off weights. Concretely, if the variance of $w_d(\mathbf{x}_i)$ or $w_c(\mathbf{x}_i)$ is large, which means that the values of contained elements are discriminative for characterizing the transferability of all $\mathbf{x}_i \in \mathcal{D}_{ood}$, then it should be paid more attention in composing the final transferability score $w(\mathbf{x}_i)$. In contrast, if the variance of $w_d(\mathbf{x}_i)$ or $w_c(\mathbf{x}_i)$ is small, then it is less helpful in evaluating the transferability of \mathbf{x}_i , so its contribution in computing $w(\mathbf{x}_i)$ should be suppressed. Mathematically, we have the following convex combination:

$$w(\mathbf{x}_i) = \frac{\text{var}(\mathbf{w}_d)}{\text{var}(\mathbf{w}_d) + \text{var}(\mathbf{w}_c)} w_d(\mathbf{x}_i) + \frac{\text{var}(\mathbf{w}_c)}{\text{var}(\mathbf{w}_d) + \text{var}(\mathbf{w}_c)} w_c(\mathbf{x}_i), \quad (12)$$

where $\text{var}(\cdot)$ denotes the variance computation regarding the input vector. Since we have re-scaled the range of these two scores $w_d(\mathbf{x}_i)$ and $w_c(\mathbf{x}_i)$ to the same level as in Eqs. (9) and (11), the variances of them can be directly employed to compare their importance in composing the transferability score $w(\mathbf{x}_i)$. Finally, we can find the transferable OOD data by weighing each OOD datum with $w(\mathbf{x}_i)$ and then perform the weighted min-max game as Eq. (6).

After the transferable OOD data have been recycled by the above weighted min-max game, their feature representations will fall into the feature space of $\mathcal{D}_l \cup \mathcal{D}_{id}$, so that they will act as ID data. Furthermore, they will be included in SSL training to improve the performance of our classification task on the interested classes.

2.3. Semi-supervised Learning

With the aforementioned OOD data detection and adversarial learning for recycling, we can take full advantage of class mismatched datasets by finding unlabeled ID data and recyclable OOD data, as well as filtering out the useless non-recyclable OOD data. Then, we can utilize the useful original labeled data, ID data, and recyclable OOD data to implement semi-supervised learning by deploying any existing SSL regularizer to the \mathcal{L}_{ssl} in Eq. (1), such as consistency loss in [22, 24, 33], virtual adversarial training loss in [28], entropy minimization in [16], and so on.

Therefore, the general framework of the TOOR algorithm can be instantiated by substituting a specified SSL

Algorithm 1 The training process for our TOOR method

Input: Labeled set $\mathcal{D}_l = \{(\mathbf{x}_1, y_1), \dots, (\mathbf{x}_l, y_l)\}$, class-mismatched unlabeled set $\mathcal{D}_u = \{\mathbf{x}_{l+1}, \dots, \mathbf{x}_{l+u}\}$.

- 1: Train feature extractor F and classifier C on labeled set \mathcal{D}_l by minimizing the supervised fidelity term in Eq. (1);
- 2: **for** $i = 1$ to MaxIter **do**
- 3: Compute assembled label prediction $\hat{\mathbf{S}}(\mathbf{x}; \tau)$ according to Eq. (4) and the stabilized softmax score $\hat{s}(\mathbf{x}) = \max_{i \in \{1, \dots, l\}} \hat{S}_i(\mathbf{x}; \tau)$;
- 4: Perform OOD data detection to find the ID dataset \mathcal{D}_{id} and OOD dataset \mathcal{D}_{ood} through Eq. (5);
- 5: Weigh each OOD datum \mathbf{x} with the transferability score $w(\mathbf{x})$ computed through Eq. (12);
- 6: OOD data recycling and network training by minimizing Eq. (1).
- 7: **end for**

Output: Discriminator parameter θ_D ; and SSL model with parameters θ_F and θ_C for classification.

regularizer \mathcal{L}_{ssl} and the weighted min-max game in Eq. (6) into the ID data exploration term and OOD data recycling term in Eq. (1). Our TOOR method is summarized in Algorithm 1. Later experiments in Section 3.1.2 will show that TOOR can enhance many typical SSL methods in the class mismatch problem and achieve encouraging performance.

3. Experiments

In this section, we conduct exhaustive experiments to validate the proposed TOOR approach. Firstly, we evaluate the performance of our method under class mismatch on every single dataset (Section 3.1). Furthermore, we evaluate the capability of TOOR under a more challenging case when the labeled and unlabeled data come from different datasets with overlapped classes (Section 3.2). Finally, detailed performance study will be provided to verify the effectiveness of OOD data detection and recycling procedures in our TOOR approach (Section 3.3).

Implementation details of TOOR. We adopt Wide ResNet-28-2 [39] as backbone network, and send the output feature of *avg-pool* layer to the discriminator. We train the network for 500,000 iterations with a batch size of 100, and adopt Adam optimizer [20] with the initial learning rate 3×10^{-4} . The threshold δ for distinguishing ID and OOD data is set to 0.9. We use a ramp-up function to gradually increase the tradeoff parameter λ and γ to conduct SSL and adversarial domain adaptation. More details on algorithm implementation are provided in **supplementary material**.

3.1. Evaluation on Single-Dataset Scenario

In this subsection, we create a class mismatch between labeled and unlabeled data in each single dataset. Specifically, we use CIFAR10 [21] and SVHN [29] datasets to construct two class-mismatched datasets, respectively. **CIFAR10** contains 50,000/10,000 training/test images from 10 classes (six animal classes and four transportation tool

classes). Here we follow [17] by randomly choosing 400 images from each of the six animal classes in the training set to form the labeled set, and picking up 20,000 training images from all ten classes to compose the unlabeled set. By this way, the images from the animal classes are ID data and those from the transportation tool classes are OOD data. **SVHN** is composed of 73,257/26,032 training/test images from ten classes “0”~“9”. We randomly choose 100 training images from each of the six classes “0”~“5” to compose the labeled set, and sample 20,000 training images from all ten classes to form the unlabeled set.

In the following, we first show that our method is superior to traditional SSL methods in handling class mismatch problem by comparing TOOR with popular SSL methods under different amounts of OOD data (Section 3.1.1). After that, we apply the TOOR framework to the aforementioned SSL methods and make comparisons with the state-of-the-art class-mismatched SSL methods (Section 3.1.2).

3.1.1 Comparison with Traditional SSL Methods

To testify the capability of TOOR for class-mismatched SSL tasks, we vary the proportion of OOD data in the unlabeled set (denoted as ζ hereinafter) to investigate the performances of various methods under different numbers of class-mismatched data. Concretely, we set ζ to $\{0\%, 25\%, 50\%, 75\%\}$ to observe the performances of TOOR and baseline methods, where $\zeta = 0\%$ means that there are no OOD data. For TOOR, we adopt Π -model as the SSL regularizer \mathcal{L}_{ssl} , and the five traditional SSL methods for comparison include Pseudo-Labeling [24], Π -model [22, 31], Temporal Ensembling [22], VAT [28], and Mean Teacher [33]. Furthermore, we also train the backbone network Wide ResNet-28-2 on labeled set to form the “Supervised” baseline. We are aware that there is another trend of SSL methods relying on data augmentation such as MixMatch [4] and ReMixMatch [3], which is orthogonal to the main contribution of this work, so here they are not included for comparison. The detailed parameter settings of the baselines are provided in **supplementary material**.

For both CIFAR10 and SVHN, we randomly select OOD data for five times under each ζ to establish the training set, and report the average test accuracies as well as the standard deviations of comparators over five independent runs. The experimental results on both datasets are shown in Figure 3. We can see that the performances of all baseline methods seriously degrade when ζ increases, as the gradually incorporated OOD data significantly mislead the training of the above SSL methods. In contrast, our method shows more stable performance than other SSL methods in both datasets, and constantly surpasses the supervised baseline, which demonstrates that TOOR successfully avoids the possible confusion brought by the OOD data in mismatched classes. Specifically, when $\zeta = 75\%$, our TOOR can still achieve 77.81% and 90.95% test accuracies on CIFAR10

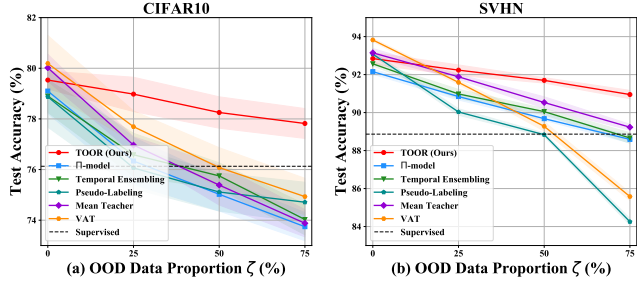


Figure 3. Test accuracies of traditional SSL methods under class mismatch with varied ζ . (a) On CIFAR10 dataset. (b) On SVHN dataset. The shaded regions with the curves indicate the standard deviations of the accuracies over five runs.

and SVHN, respectively, which are significantly higher than 74.93% and 89.23% achieved by the second best method.

3.1.2 Comparison with Class-Mismatched SSL Methods

In this part, we apply the proposed TOOR framework to some typical SSL methods (*e.g.*, Pseudo-Labeling [24], Π-model [22, 31], Temporal Ensembling [22], VAT [28], and Mean Teacher [33]) to enable them to handle class-mismatched cases, and compare them with two existing optimal approaches (*i.e.*, UASD [9] and DS³L [17]) that deal with class-mismatched SSL problem. Similar to Section 3.1.1, we also investigate the results of various methods under $\zeta = \{0\%, 25\%, 50\%, 75\%\}$, and the average accuracies of five runs on CIFAR10 and SVHN datasets are shown in Figure 4. We can see that all the five traditional SSL methods combined with TOOR (*i.e.*, “Π-model+TOOR”, “Temporal Ensembling+TOOR”, “Pseudo-Labeling+TOOR”, “Mean Teacher+TOOR”, and “VAT+TOOR”) perform satisfactorily, and the significant performance drop revealed by Figure 3 does not appear anymore, which indicates that TOOR is quite general and can help many traditional SSL methods to tackle the class mismatch problem. Moreover, the five SSL methods enhanced by TOOR outperform UASD and DS³L in most cases, which again demonstrates the effectiveness of our method. Specifically, when $\zeta = 50\%$ which means half of the unlabeled images are OOD data, our “Mean teacher + TOOR” achieves the accuracy of 78.88%, which is much higher than UASD and DS³L with the accuracies 77.10% and 77.22% correspondingly on CIFAR10 dataset. On SVHN dataset, the accuracy of “Mean teacher + TOOR” is as high as 92.39%, which outperforms UASD and DS³L with the accuracies 90.68% and 90.59% accordingly.

3.2. Evaluation on Cross-Dataset Scenario

To further test the effectiveness of our proposed method, we create a more challenging scenario when labeled and unlabeled data come from two different datasets with overlapped classes, which contains a much larger distribution gap between labeled and unlabeled data than the single-dataset scenario conducted in Section 3.1. In our ex-

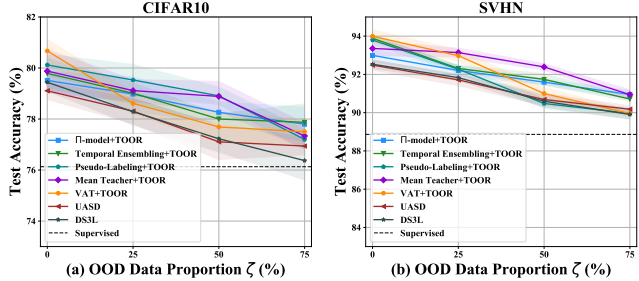


Figure 4. Test accuracies of various class-mismatched SSL methods under class mismatch with varied ζ . (a) On CIFAR10 dataset. (b) On SVHN dataset. The shaded regions with the curves indicate the standard deviations of the accuracies over five runs.

periments, we choose CIFAR100 [21] and ImageNet [10] to form our labeled and unlabeled set, respectively. **CIFAR100** has the same image data as CIFAR10 but contains 100 fine-grained classes. **ImageNet** contains 1,331,167 images from 1,000 classes. To create the dataset for evaluation, we choose 6,000 images from 60 classes in CIFAR100 as the labeled set where the selected 60 classes can also be found in ImageNet. Then we sample 20,000 images from 100 classes in CIFAR100 to form the unlabeled set, which contains the 60 classes that correspond to the chosen classes in the labeled set. Besides, the remaining 40 classes in the unlabeled set are randomly selected from the rest 940 classes in ImageNet. Here we denote the established dataset as “CIFAR100+ImageNet”, more details on dataset establishment are provided in **supplementary material**.

For all experiments conducted in this subsection, we set the OOD proportion $\zeta = 50\%$ and adopt Π-model as the backbone method. The experimental results are shown in Table 1. We can see that TOOR outperforms all the other compared methods on the constructed dataset, which indicates the capability of TOOR in tackling challenging classification task under large class mismatch. Specifically, TOOR significantly surpasses the supervised baseline with 2.59% on the averaged test accuracy while all the other compared methods show performance degradation than the supervised baseline. This is due to the large distribution shift between labeled and unlabeled data, which makes the original unlabeled ID data harmful to the performance of SSL. Thanks to the introduced transferring strategy, the proposed TOOR method can successfully eliminate the distribution gap via using adversarial learning, therefore achieving an improved performance than the supervised baseline.

3.3. Performance Study

From the above experimental results presented in Sections 3.1 and 3.2, we can see that TOOR achieves very encouraging results. Here we further analyze the effects of key components in TOOR, and study the behind reasons for TOOR in achieving good performance. Specifically, we see that the OOD data detection in Section 2.1 and transferable OOD data recycling in Section 2.2 are critical to tackling

Table 1. Test accuracies (%) with standard deviations over five runs on CIFAR100+ImageNet dataset. The best results are highlighted in **bold**.

Method	CIFAR100 + ImageNet
Supervised	45.31 ± 1.12
Pseudo-Labeling [24]	43.90 ± 0.46
II-model [22, 31]	43.81 ± 1.28
Temporal Ensembling [22]	44.10 ± 0.31
VAT [28]	44.49 ± 0.69
Mean Teacher [33]	43.23 ± 0.84
UASD [9]	44.90 ± 0.47
DS ³ L [17]	45.10 ± 1.25
TOOR (Ours)	47.90 ± 0.84

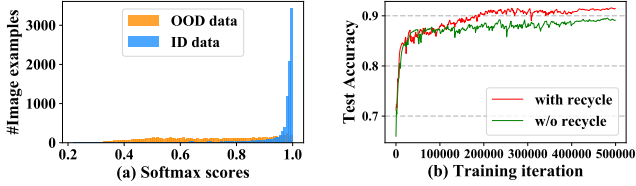


Figure 5. (a) Histogram of the computed softmax scores $\hat{s}(x)$ over all unlabeled images when supervised training finishes. (b) Test accuracies of different model configurations. Red curve: training with OOD data recycling. Green curve: training without recycling.

the class mismatch problem and boosting the performance, so next we validate their effectiveness, respectively. In the main paper, we only report the experimental results on SVHN with $\zeta = 0.5$ and use II-model as backbone method. More results on CIFAR10 and CIFAR100+ImageNet are referred to **supplementary material**.

OOD data detection. As mentioned in Section 2.1, The performance of OOD data detection largely depends on the stabilized softmax scores. To show the reasonability of our softmax scores, we plot the scores of ID and OOD data in Figure 5 (a). It is noteworthy that most of ID data have scores close to 1, and the scores of OOD data show an uniform distribution as most of them are left out from the network training. Therefore, the computed softmax score provides valuable information in discriminating ID data and OOD data. As a result, we use a relatively large value 0.9 as the threshold δ to guarantee that all decided ID data are correct, as the current excluded ID data are also possible to be recalled by the subsequent recycling procedure. However, if we use 0.5 as the threshold δ , the erroneously incorporated non-recyclable OOD data will never have a chance to be discarded, which may further hurt the performance.

OOD data recycling. To further study the contributions of the recycling procedure, we compare the experimental results obtained by training our method with and without recycling. The results are shown in Figure 5 (b), which reveals that the recycling process is beneficial for our TOOR method to enhance the classification performance.

Furthermore, we provide the visualization of the image features extracted by Wide ResNet-28-2 via using t-SNE method [27] in Figure 6. It can be observed that most of the

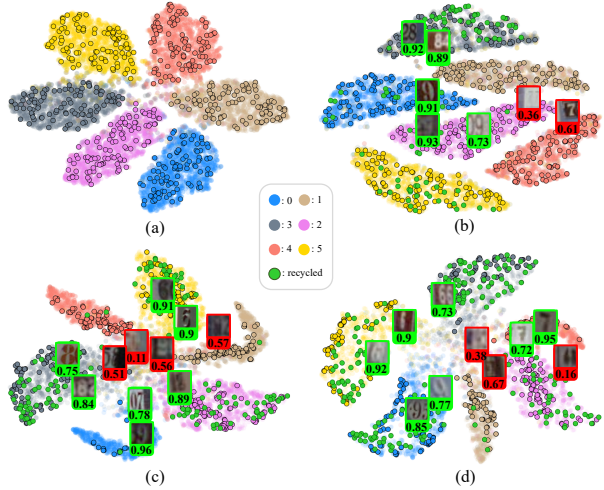


Figure 6. t-SNE visualizations of the image representations. Figures (a)~(d) correspond to the results obtained on SVHN with ζ equaling 0%, 25%, 50%, 75%, respectively. Different colors denote the image data from different classes, where the green dots indicate the recycled OOD data determined by TOOR, and the dots with black boundary denote the originally labeled data. Besides, some of the recyclable OOD images (green boxes) and non-recyclable OOD images (red boxes) are visualized, of which the transferability scores $w(x)$ are also indicated below the images.

recycled OOD data (see the green dots) with relatively large transferability scores lie in the dense region within each cluster, while those with small transferability scores are distributed in a scattered way. Besides, we can see that the recycled OOD image data show great similarity to the classes in the labeled set. For example, we can see that many OOD data corresponding to digit “9” are mapped to the ID data with class “0”, as these two digits look similarly. In contrast, we can see that most of the non-recyclable OOD data in the red boxes are blurry and some of them cannot be recognized even by human. Hence, our method managed to alleviate the negative influence of these non-recyclable OOD data by assigning them with small transferability scores. In a word, our strategy of utilizing transferability to characterize recyclability makes sense, which is helpful to find the potential useful OOD data.

4. Conclusion

In this paper, we propose a novel SSL method termed TOOR that solves the class mismatch problem. Concretely, instead of discarding or down-weighting all the detected OOD data, we adaptively weigh all OOD data by quantifying their transferability to find the transferable subset, which can be further recycled via adversarial domain adaptation. As a result, the recycled OOD data can be re-used to help to train a better semi-supervised classifier than existing methods. The comparison results with various SSL methods on benchmark datasets demonstrate the effectiveness of our proposed TOOR in handling class mismatch problems.

Supplementary Material

In this supplementary material, we first provide the implementation details of our TOOR method and the baseline methods in Section A. Then we will explain the dataset establishment in Section B. Finally, we present the additional experimental results in Section C, which includes the evaluation of our TOOR method on CIFAR100 and ImageNet datasets, as well as the performance study on CIFAR10 and CIFAR100+ImageNet datasets.

A. Implementation Details

All the investigated algorithms are implemented by using the batch size of 100, and are trained for 500,000 iterations. The network training for all methods is conducted by Adam optimizer [20] with the weight decay factor 0.2 after 400,000 iterations. Other implementation details for each of them are presented below.

A.1. The Proposed TOOR

Here we present the configurations of our TOOR by specifying the network architectures as well as the hyperparameter values.

Backbone network F . We choose the Wide ResNet-28-2 [39] as our backbone network F , and consider the last fully connected layer followed by a softmax operation as the classifier C . The architecture of the adopted Wide ResNet-28-2 is shown in Table 2. To achieve a fair comparison, we implement all other methods by using the same backbone network as our TOOR method.

Discriminator D . We choose the same structure as in [7] to construct our discriminator, which is shown in Table 3. The flip-coefficient $flip_coeff$ in the GRL [11] aims to suppress the noisy signals from the discriminator at the early stages of training procedure, which ramps up from 0 to 1 by following the function $flip_coeff = \frac{2}{1+\exp(-10 \times (iter - pretrain_iter) \times \frac{1}{400,000})} - 1$, where $iter$ denotes the current training iteration, $pretrain_iter$ denotes the number of iterations for supervised training and is set to 5,000 in our experiments. The ramp up curve is shown in Figure 7 (a).

Hyperparameters. We set the temperature τ in Eq. (2) of our main paper as 0.8 to compute the softmax scores, and set the OOD data detection threshold δ as 0.9 for SVHN and CIFAR10 datasets to distinguish ID data from OOD data. For CIFAR100 and ImageNet datasets, we set δ to 0.8. The trade-off parameters λ and γ ramp up from 0 to 1 by following the functions $\lambda = \exp(-5 \times (1 - \min(\frac{iter}{200,000}, 1))^2)$ and $\gamma = \exp(-5 \times (1 - \min(\frac{iter}{400,000}, 1))^2)$, respectively, of which the variations are shown in Figure 7 (b). Since our method is a general framework which can be applied to many traditional SSL methods, we use different initial

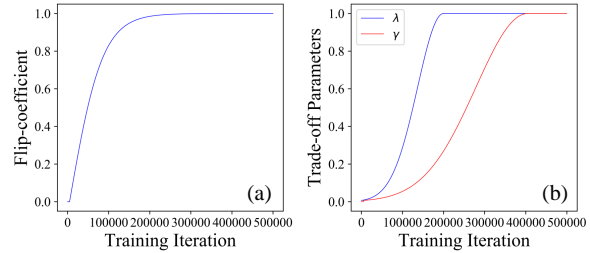


Figure 7. The ramp up curves of different parameters. (a) flip-coefficient $flip_coeff$. (b) trade-off parameters λ and γ .

learning rates for our backbone network by following the original settings of the adopted SSL methods. The detailed configurations are shown in Table 4. For discriminator D , we set the initial learning rate to 0.001.

A.2. Baseline Methods

For our compared baseline methods, we explain the details of the included traditional SSL methods as well as the class-mismatched SSL methods.

Traditional SSL methods. For traditional SSL method including Pseudo-Labeling [24], Π -model [22, 31], Temporal Ensembling [22], VAT [28], and Mean Teacher [33], we follow [30] and train the network by using different hyperparameter settings regarding the learning rate, decay schedule, and weight decay coefficients. The hyperparameter settings are summarized in Table 4.

Class-mismatched SSL methods. The compared class-mismatched SSL methods include UASD [9] and DS³L [17]. For UASD, we choose the ensemble size of the network predictions as 10, and set the OOD filter threshold as the average value of the confidence scores regarding all ID data in the validation set. For DS³L, we show the architecture of its weighting network in Table 5. Note that the meta network has the same architecture as its backbone network, which is shown in Table 2. The detailed hyperparameters of UASD and DS³L are also listed in Table 4.

B. Dataset Establishment

In this paper, we have used CIFAR10 [21], SVHN [29], CIFAR100 [21], and ImageNet [10] datasets to evaluate the performance of our TOOR method. In the following, we will present the detailed dataset establishment based on these datasets, which includes the single-dataset scenario and the cross-dataset scenario mentioned in Section 3.2 in the main paper.

For the single-dataset scenario, we have presented the evaluation results of various methods on CIFAR10 and SVHN datasets in the main paper. Specifically, **CIFAR10** contains 50,000 and 10,000 natural images with the size of 32×32 for training and testing accordingly, which consist of six animal classes (e.g., “bird”, “cat”, “deer”, “dog”, “frog”,

Table 2. Architecture of backbone network F .

Group Name	Layer	Hyperparameters
	Input	32×32 RGB image
	Translation	Randomly $\{\Delta x, \Delta y\} \sim [-2, 2]$
	Horizontal flip [*]	Randomly $p = 0.5$
	Gaussian noise	$\sigma = 0.15$
conv1	Convolutional	16 filters, conv 3×3
conv2	Batch-Normalization Leaky-ReLU Convolutional Batch-Normalization Leaky-ReLU Convolutional	$momentum = 1 \times 10^{-3}$ $negative_slope = 0.1$ 32 filters, conv 3×3 $momentum = 1 \times 10^{-3}$ $negative_slope = 0.1$ 32 filters, conv 3×3
conv3	Batch-Normalization Leaky-ReLU Convolutional Batch-Normalization Leaky-ReLU Convolutional	$momentum = 1 \times 10^{-3}$ $negative_slope = 0.1$ 64 filters, conv 3×3 $momentum = 1 \times 10^{-3}$ $negative_slope = 0.1$ 64 filters, conv 3×3
conv4	Batch-Normalization Leaky-ReLU Convolutional Batch-Normalization Leaky-ReLU Convolutional	$momentum = 1 \times 10^{-3}$ $negative_slope = 0.1$ 128 filters, conv 3×3 $momentum = 1 \times 10^{-3}$ $negative_slope = 0.1$ 128 filters, conv 3×3
avg-pool	Batch-Normalization Leaky-ReLU Average Pooling	$momentum = 1 \times 10^{-3}$ $negative_slope = 0.1$ $outputsize = 1$
	Fully Connected Softmax	$classes = 6$

^{*} Not applied on SVHN experiments.

Table 3. Architecture of our discriminator D .

Layer	Hyperparameters
GRL	flip-coefficient
Linear	$128 \rightarrow 1,024$
ReLU	
Dropout	$p = 0.5$
Linear	$1,024 \rightarrow 1,024$
ReLU	
Dropout	$p = 0.5$
Linear	$1,024 \rightarrow 1$
Sigmoid	

and “horse”) and four transportation tool classes (e.g., “airplane”, “automobile”, “ship”, and “truck”). Here we follow [17] by randomly choosing 400 images from each of the six animal classes in the training set to construct the labeled set, and picking up 20,000 training images from all ten classes to compose the unlabeled set. In this way, the images belonging to the animal classes are ID data and those from the transportation tool classes are OOD data. **SVHN** is composed of 73,257 training images and 26,032 test images

with the resolution of 32×32 , which are collected from real-world house numbers. This dataset contains ten classes, namely the ten digits “0”~“9”. We randomly choose 100 images from the each of six classes “0”~“5” in the training set to compose the labeled set, and randomly sample 20,000 training images from all ten classes “0”~“9” to form the unlabeled set.

Furthermore, in Section C.1 of this supplementary material, we will present the evaluation results of various methods on CIFAR100 and ImageNet. Concretely, **CIFAR100** has the same numbers of training and test images as CIFAR10 with the same size, but contains 100 fine-grained classes. Here we choose 100 training images from each of the first 60 classes (“0”~“59”) to construct the labeled set, and pick up 20,000 training images from all 100 classes to compose the unlabeled set. **ImageNet** is a downsampled version of the original ImageNet dataset with the size of 32×32 , it contains 1,281,167 training images and 50,000 validation images from 1,000 classes. Similar to CIFAR100, we choose 100 training images from the first 60 classes (“0”~“59”) to construct the labeled set, and

Table 4. Hyperparameter settings of the compared SSL methods.

Shared		
learning rate decay factor	0.2	
# training iteration in which learning rate decay starts	400,000	
# training iteration in which consistency coefficient ramp up starts	200,000	
Supervised		
Initial learning rate	0.003	
II-Model [22, 31]		
Initial learning rate	3×10^{-4}	
Max consistency coefficient	20	
Temporal Ensembling [22]		
Initial learning rate	3×10^{-4}	
Max consistency coefficient	20	
Exponential moving average factor	0.6	
Mean Teacher [33]		
Initial learning rate	4×10^{-4}	
Max consistency coefficient	8	
Exponential moving average decay	0.95	
VAT [28]		
Initial learning rate	0.003	
Max consistency coefficient	0.3	
ϵ	6.0 or 1.0*	
ξ	10^{-6}	
Pseudo-Labeling [24]		
Initial learning rate	0.003	
Max consistency coefficient	0.3	
Pseudo-Labeling threshold	0.95	
UASD [9]		
Initial learning rate	0.003	
Ensemble size	10	
DS ³ L [17]		
Initial learning rate for backbone network	0.003	
Initial learning rate for meta network	0.001	
Initial learning rate for weighting network	6×10^{-5}	

* 6.0 for CIFAR10 dataset and 1.0 for SVHN dataset.

Table 5. Architecture of the weighting network in DS³L.

Layer	Hyperparameters
Linear	6→100
ReLU	
Linear	100→1
Sigmoid	

pick up 20,000 training images from the first 100 classes (“0”~“99”) to compose the unlabeled set.

For the cross-dataset scenario, we randomly choose 100 training images from each of the 60 classes in CIFAR100 as the labeled set, where the selected 60 classes can also

be found in ImageNet. Then we sample 20,000 images from 100 classes in ImageNet to form the unlabeled set, which contains the 60 classes that correspond to the chosen classes in the labeled set. Besides, the remaining 40 classes in the unlabeled set are randomly selected from the rest 940 classes in ImageNet. Here we show the mapping of the 60 shared classes from CIFAR100 to ImageNet in Table 6. According to the presented class name of each class, we can see that many of the shared classes from CIFAR100 and ImageNet are not strictly identical, hence introducing a distribution gap between the labeled data and unlabeled data.

Table 6. Mapping of the 60 shared classes from CIFAR100 to ImageNet. “class name” denotes the description of each class in the dataset, and “#” denotes the corresponding label.

CIFAR100		ImageNet		CIFAR100		ImageNet	
class name	#	class name	#	class name	#	class name	#
aquarium fish	1	goldfish, <i>Carassius auratus</i>	1	lion	43	cougar, puma, catamount...	286
bear	3	koala, koala bear, kangaroo bear...	105	lizard	44	whiptail, whiptail lizard	41
beaver	4	beaver	337	lobster	45	American lobster, Northern lobster...	122
bed	5	studio couch, day bed	831	mushroom	51	mushroom	947
bee	6	bee	309	orange	53	orange	950
beetle	7	tiger beetle	300	otter	55	otter	360
bicycle	8	bicycle-built-for-two, tandem...	444	pickup truck	58	pickup, pickup truck	717
bottle	9	beer bottle	440	plate	61	plate	923
bowl	10	mixing bowl	659	porcupine	63	porcupine, hedgehog	334
bridge	12	steel bridge, arch bridge	821	rabbit	65	wood rabbit, cottontail...	330
bus	13	school bus	779	ray	67	electric ray, crampfish, numbfish...	5
butterfly	14	ringlet, ringlet butterfly	322	shark	73	great white shark, white shark...	2
camel	15	Arabian camel, dromedary...	354	skunk	75	skunk, polecat, wood pussy	361
can	16	milk can	653	snail	77	snail	113
castle	17	castle	483	snake	78	ringneck snake, ring-necked snake...	53
chair	20	barber chair	423	spider	79	wolf spider, hunting spider	77
chimpanzee	21	chimpanzee, chimp, pan troglodytes	367	squirrel	80	fox squirrel, eastern fox squirrel...	335
clock	22	analog clock	409	streetcar	81	streetcar, tram, tramcar...	829
cockroach	24	cockroach, roach	314	table	84	dining table, board	532
crab	26	dungeness crab, cancer magister	118	tank	85	tank, army tank...	847
crocodile	27	African crocodile, Nile crocodile...	49	telephone	86	dial telephone, dial phone	528
cup	28	cup	968	television	87	television, television system	851
elephant	31	Indian elephant, <i>Elephas maximus</i>	385	tiger	88	tiger, <i>Panthera tigris</i>	292
fox	34	grey fox, gray fox...	280	tractor	89	tractor	866
hamster	36	hamster	333	train	90	bullet train, bullet	466
house	37	restaurant, eating house...	762	turtle	93	loggerhead, loggerhead turtle...	33
kangaroo	38	wallaby, brush kangaroo	104	wardrobe	94	wardrobe, closet, press	894
keyboard	39	typewriter keyboard	878	whale	95	grey whale, gray whale, devilfish...	147
lamp	40	table lamp	846	wolf	97	timber wolf, grey wolf...	269
leopard	42	leopard, <i>Panthera pardus</i>	288	worm	99	nematode, nematode worm...	111

C. Additional Experiments

Here we provide additional experimental results to further testify the effectiveness of the proposed method, which includes the evaluation on CIFAR100 and ImageNet datasets, as well as the performance study on CIFAR10 and CIFAR100+ImageNet datasets.

C.1. Evaluation on CIFAR100 and ImageNet datasets

Given the established CIFAR100 and ImageNet datasets, we choose II-model as the backbone method, and set $\zeta = 50\%$ to compare TOOR with traditional SSL methods as well as the class-mismatched SSL methods. The experimental results are presented in Table 7. We can see that our method outperforms all other compared methods on the established CIFAR100 and ImageNet datasets, which indicates the capability of TOOR on tackling challenging classification tasks under class mismatch.

Table 7. Test accuracies (%) with standard deviations over five runs on CIFAR100 and ImageNet datasets. The best results are highlighted in **bold**.

Method	CIFAR100	ImageNet
Supervised	52.94 ± 0.84	41.26 ± 0.40
Pseudo-Labeling [24]	52.73 ± 1.12	41.04 ± 1.08
II-model [22, 31]	52.11 ± 0.70	41.01 ± 1.03
Temporal Ensembling [22]	52.84 ± 0.55	41.48 ± 0.51
VAT [28]	51.93 ± 2.18	42.16 ± 0.42
Mean Teacher [33]	53.10 ± 0.36	41.45 ± 0.98
UASD [9]	54.07 ± 0.56	42.07 ± 1.04
DS ³ L [17]	54.14 ± 0.63	41.39 ± 0.93
TOOR (Ours)	55.83 ± 1.19	42.63 ± 1.01

C.2. Performance Study

In our main paper, we only provide the performance study results of our method on SVHN dataset. In this section, we follow the similar way as in the main paper

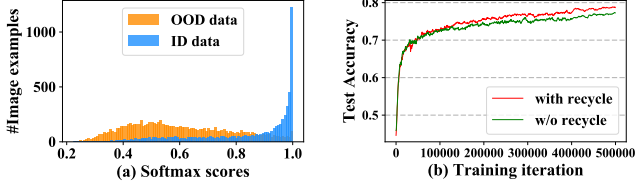


Figure 8. Performance study on CIFAR10 dataset. (a) Histogram of the computed softmax scores $\hat{s}(x)$ over all unlabeled images when supervised training finishes. (b) Test accuracies of different model configurations. Red curve: training with OOD data recycling. Green curve: training without recycling.

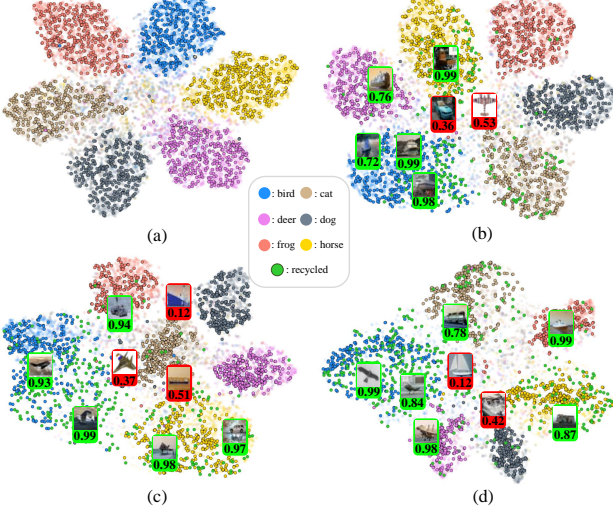


Figure 9. t-SNE visualizations of the image representations. Figures (a)~(d) correspond to the results obtained on CIFAR10 dataset with OOD data proportion ζ equaling 0%, 25%, 50%, 75%, respectively. Different colors denote the image data from different classes, where the green dots indicate the recycled OOD data determined by TOOR, and the dots with black boundary denote the originally labeled data. Besides, some of the recyclable OOD images (green boxes) and non-recyclable OOD images (red boxes) are visualized, of which the transferability scores $w(x)$ are also indicated below the images.

to conduct the performance study on CIFAR10 and CIFAR100+ImageNet dataset, which both include the investigations on the effectiveness of OOD data detection and OOD data recycling. Note that the number of classes in CIFAR100+ImageNet dataset is quite large which makes the illustration of the image features not feasible, hence we will not present the t-SNE visualization of TOOR on this dataset.

C.2.1 CIFAR10 dataset

OOD data detection. To show the reasonability of the computed softmax scores, we plot the scores of ID data and OOD data from CIFAR10 dataset in Figure 8 (a). We can see a similar result as in the main paper, which indicates that our computed softmax score provides a valuable clue

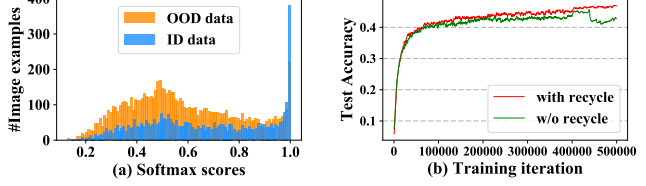


Figure 10. Performance study on CIFAR100+ImageNet dataset. (a) Histogram of the computed softmax scores $\hat{s}(x)$ over all unlabeled images when supervised training finishes. (b) Test accuracies of different model configurations. Red curve: training with OOD data recycling. Green curve: training without recycling.

for distinguishing ID data from OOD data.

OOD data recycling. We also conduct similar experiments as in the main paper by comparing the performance obtained by training our method with and without recycling, and the results are shown in Figure 8 (b). We can see that the recycling procedure can promote the performance of our method in the later stage of network training, which indicates that the recycling process is beneficial for our TOOR method to tackle the class mismatch problem.

Furthermore, we present the t-SNE visualization of image features from CIFAR10 dataset in Figure 9. We can see that most of the recycled OOD data (see the green dots) with relatively large transferability scores lie in the dense region within each cluster, while those with small transferability scores are distributed in a scattered way, which is consistent with the results in the main paper. Moreover, we can also see that the recycled OOD images show great similarity to the classes in the labeled set. For example, some of the “airplane” images are recycled to the “bird” classes, as they have similar shapes. On the other hand, some of the images show less similarity to the animal classes are assigned with small transferability scores, such as “0.12” and “0.42”. To sum up, our strategy of utilizing transferability to characterize recyclability is still applicable in CIFAR10 dataset and helps to exploit the potential information inherited by OOD data in the mismatched classes.

C.2.2 CIFAR100+ImageNet dataset

OOD data detection. To validate the OOD data detection performance on the cross-dataset scenario, we plot the scores of ID data and OOD data from CIFAR100+ImageNet dataset in Figure 10 (a), we can see that most of the scores of ID data are still larger than the scores of OOD data in such challenging scenario, hence the computed softmax score can still be a satisfactory criterion for distinguishing ID data from OOD data.

OOD data recycling. Here we compare the performance obtained by training our method with and without recycling on CIFAR100+ImageNet dataset, and the results are shown in Figure 10 (b). We see that the recycling procedure is still helpful for network training. Moreover, we find that when

training without recycling, a sudden performance drop appears at the later stage of training. This is because that the unlabeled data may mislead the learning process, and the learned classifier will overfit to the biased unlabeled data. However, the recycling procedure can eliminate the distribution gap between labeled and unlabeled data and enhance the generalizability of the learned classifier, thus greatly preventing the performance drop and achieving a satisfactory result.

References

- [1] Mikhail Belkin, Partha Niyogi, and Vikas Sindhwani. Manifold regularization: A geometric framework for learning from labeled and unlabeled examples. *Journal of Machine Learning Research (JMLR)*, 7(Nov):2399–2434, 2006. 3
- [2] Kristin P Bennett and Ayhan Demiriz. Semi-supervised support vector machines. In *NeurIPS*, pages 368–374, 1999. 1
- [3] David Berthelot, Nicholas Carlini, Ekin D. Cubuk, Alex Kurakin, Kihyuk Sohn, Han Zhang, and Colin Raffel. Remixmatch: Semi-supervised learning with distribution alignment and augmentation anchoring. *arXiv preprint arXiv:1911.09785*, 2019. 6
- [4] David Berthelot, Nicholas Carlini, Ian Goodfellow, Nicolas Papernot, Avital Oliver, and Colin A Raffel. Mixmatch: A holistic approach to semi-supervised learning. In *NeurIPS*, pages 5049–5059, 2019. 1, 6
- [5] Avrim Blum and Tom Mitchell. Combining labeled and unlabeled data with co-training. In *COLT*, pages 92–100, 1998. 1
- [6] Zhangjie Cao, Lijia Ma, Mingsheng Long, and Jianmin Wang. Partial adversarial domain adaptation. In *ECCV*, pages 135–150, 2018. 2, 4
- [7] Zhangjie Cao, Kaichao You, Mingsheng Long, Jianmin Wang, and Qiang Yang. Learning to transfer examples for partial domain adaptation. In *CVPR*, pages 2985–2994, 2019. 2, 4, 9
- [8] Olivier Chapelle, Bernhard Scholkopf, and Alexander Zien. Semi-supervised learning. *IEEE Transactions on Neural Networks and Learning Systems (TNNLS)*, 20(3):542–542, 2009. 1
- [9] Yanbei Chen, Xiatian Zhu, Wei Li, and Shaogang Gong. semi-supervised learning under class distribution mismatch. In *AAAI*, pages 3569–3576, 2020. 2, 7, 8, 9, 11, 12
- [10] Patryk Chrabaszcz, Ilya Loshchilov, and Frank Hutter. A downsampled variant of imagenet as an alternative to the cifar datasets. *arXiv preprint arXiv:1707.08819*, 2017. 7, 9
- [11] Yaroslav Ganin and Victor Lempitsky. Unsupervised domain adaptation by backpropagation. In *ICML*, pages 1180–1189. PMLR, 2015. 3, 9
- [12] Yaroslav Ganin, Evgeniya Ustinova, Hana Ajakan, Pascal Germain, Hugo Larochelle, Fran ois Laviolette, Mario Marchand, and Victor Lempitsky. Domain-adversarial training of neural networks. *Journal of Machine Learning Research (JMLR)*, 17(1):2096–2030, 2016. 2, 4
- [13] Bo Geng, Dacheng Tao, Chao Xu, Linjun Yang, and Xian-Sheng Hua. Ensemble manifold regularization. *IEEE Transactions on Pattern Analysis and Machine Intelligence (TPAMI)*, 34(6):1227–1233, 2012. 3
- [14] Chen Gong, Tongliang Liu, Dacheng Tao, Keren Fu, Enmei Tu, and Jie Yang. Deformed graph laplacian for semisupervised learning. *IEEE Transactions on Neural Networks and Learning Systems (TNNLS)*, 26(10):2261–2274, 2015. 1
- [15] Ian Goodfellow, Jean Pouget-Abadie, Mehdi Mirza, Bing Xu, David Warde-Farley, Sherjil Ozair, Aaron Courville, and Yoshua Bengio. Generative adversarial nets. In *NeurIPS*, pages 2672–2680, 2014. 4
- [16] Yves Grandvalet and Yoshua Bengio. Semi-supervised learning by entropy minimization. In *NeurIPS*, pages 529–536, 2005. 1, 5
- [17] Lan-Zhe Guo, Zhen-Yu Zhang, Yuan Jiang, Yu-Feng Li, and Zhi-Hua Zhou. Safe deep semi-supervised learning for unseen-class unlabeled data. In *ICML*, 2020. 2, 6, 7, 8, 9, 10, 11, 12
- [18] Geoffrey Hinton, Oriol Vinyals, and Jeff Dean. Distilling the knowledge in a neural network. *arXiv preprint arXiv:1503.02531*, 2015. 3
- [19] Ahmet Iscen, Giorgos Tolias, Yannis Avrithis, and Ondrej Chum. Label propagation for deep semi-supervised learning. In *CVPR*, pages 5070–5079, 2019. 1
- [20] Diederik P Kingma and Jimmy Ba. Adam: A method for stochastic optimization. *arXiv preprint arXiv:1412.6980*, 2014. 6, 9
- [21] Alex Krizhevsky, Geoffrey Hinton, et al. Learning multiple layers of features from tiny images. 2009. 6, 7, 9
- [22] Samuli Laine and Timo Aila. Temporal ensembling for semi-supervised learning. In *ICLR*, 2016. 1, 3, 4, 5, 6, 7, 8, 9, 11, 12
- [23] Yann LeCun, Yoshua Bengio, and Geoffrey Hinton. Deep learning. *nature*, 521(7553):436–444, 2015. 1
- [24] Dong-Hyun Lee. Pseudo-label: The simple and efficient semi-supervised learning method for deep neural networks. In *ICML Workshop*, volume 3, 2013. 1, 5, 6, 7, 8, 9, 11, 12
- [25] Shiyu Liang, Yixuan Li, and Rayadurgam Srikant. Enhancing the reliability of out-of-distribution image detection in neural networks. In *ICLR*, 2018. 3, 4
- [26] Yucen Luo, Jun Zhu, Mengxi Li, Yong Ren, and Bo Zhang. Smooth neighbors on teacher graphs for semi-supervised learning. In *CVPR*, pages 8896–8905, 2018. 1
- [27] Laurens van der Maaten and Geoffrey Hinton. Visualizing data using t-sne. *Journal of Machine Learning Research (JMLR)*, 9(Nov):2579–2605, 2008. 8
- [28] Takeru Miyato, Shin-ichi Maeda, Masanori Koyama, and Shin Ishii. Virtual adversarial training: a regularization method for supervised and semi-supervised learning. *IEEE Transactions on Pattern Analysis and Machine Intelligence (TPAMI)*, 41(8):1979–1993, 2018. 1, 2, 5, 6, 7, 8, 9, 11, 12
- [29] Yuval Netzer, Tao Wang, Adam Coates, Alessandro Bissacco, Bo Wu, and Andrew Y Ng. Reading digits in natural images with unsupervised feature learning. In *NeurIPS Workshop*, 2011. 6, 9
- [30] Avital Oliver, Augustus Odena, Colin A Raffel, Ekin Dogus Cubuk, and Ian Goodfellow. Realistic evaluation of deep semi-supervised learning algorithms. In *NeurIPS*, pages 3235–3246, 2018. 1, 9

- [31] Mehdi Sajjadi, Mehran Javanmardi, and Tolga Tasdizen. Regularization with stochastic transformations and perturbations for deep semi-supervised learning. In *NeurIPS*, pages 1163–1171, 2016. 6, 7, 8, 9, 11, 12
- [32] Kihyuk Sohn, David Berthelot, Chun-Liang Li, Zizhao Zhang, Nicholas Carlini, Ekin D Cubuk, Alex Kurakin, Han Zhang, and Colin Raffel. Fixmatch: Simplifying semi-supervised learning with consistency and confidence. *arXiv preprint arXiv:2001.07685*, 2020. 1
- [33] Antti Tarvainen and Harri Valpola. Meanteachers are better role models: Weight-averaged consistency targets improve semi-supervised deep learning results. In *NeurIPS*, pages 1195–1204, 2017. 1, 2, 3, 5, 6, 7, 8, 9, 11, 12
- [34] Eric Tzeng, Judy Hoffman, Kate Saenko, and Trevor Darrell. Adversarial discriminative domain adaptation. In *CVPR*, pages 7167–7176, 2017. 2, 4
- [35] Fei Wang and Changshui Zhang. Label propagation through linear neighborhoods. *IEEE Transactions on Knowledge and Data Engineering (TKDE)*, 20(1):55–67, 2007. 1
- [36] Qin Wang, Wen Li, and Luc Van Gool. Semi-supervised learning by augmented distribution alignment. In *ICCV*, pages 1466–1475, 2019. 1
- [37] Yao Yao, Jiehui Deng, Xiuhua Chen, Chen Gong, Jianxin Wu, and Jian Yang. Deep discriminative CNN with temporal ensembling for ambiguously-labeled image classification. In *AAAI*, 2020. 5
- [38] Bing Yu, Jingfeng Wu, Jinwen Ma, and Zhanxing Zhu. Tangent-normal adversarial regularization for semi-supervised learning. In *CVPR*, pages 10676–10684, 2019. 3
- [39] Sergey Zagoruyko and Nikos Komodakis. Wide residual networks. In *BMVC*, 2016. 6, 9
- [40] Xiaohua Zhai, Avital Oliver, Alexander Kolesnikov, and Lucas Beyer. S4l: Self-supervised semi-supervised learning. In *ICCV*, pages 1476–1485, 2019. 1
- [41] Jing Zhang, Zewei Ding, Wanqing Li, and Philip Ogunbona. Importance weighted adversarial nets for partial domain adaptation. In *CVPR*, 2018. 2, 4
- [42] Liheng Zhang and Guo-Jun Qi. Wcp: Worst-case perturbations for semi-supervised deep learning. In *CVPR*, pages 3912–3921, 2020. 1
- [43] Dengyong Zhou, Olivier Bousquet, Thomas N Lal, Jason Weston, and Bernhard Schölkopf. Learning with local and global consistency. In *NeurIPS*, pages 321–328, 2004. 1